Journal of Materials Research and Technology 33 (2024) 2756–2763

Contents lists available at ScienceDirect

Journal of Materials Research and Technology

journal homepage: www.elsevier.com/locate/jmrt

Enhancing filler ratio and thermal conductivity of polyphenylene sulfide composites using molybdenum sulfide and carbon nanotubes: A layer-by-layer hot-pressing approach

Minsu Kim [a], Jooheon Kim [a,b,*]

[a] School of Chemical Engineering, Chung-Ang University, Seoul, 06974, Republic of Korea
[b] Department of Intelligent Energy and Industry, Graduate School, Chung-Ang University, Seoul, 06974, Republic of Korea

ARTICLE INFO

Handling editor: SN Monteiro

Keywords:
Polyphenylene sulfide
Molybdenum sulfide
Carbon nanotube
Thermal conductivity
Layered structure

ABSTRACT

In this study, we aimed to address challenges in thermal management and structural applications by developing composite materials with enhanced thermal conductivity and insulation properties. Our approach involved combining two-dimensional MoS_2 nanosheets with carbon nanotubes (CNTs), leveraging their respective properties to create synergistic effects. MoS_2, renowned for its remarkable electrical and mechanical attributes, was synthesized via a hydrothermal reaction and subsequently exfoliated using liquid-phase exfoliation techniques. Meanwhile, CNTs were surface-treated to prevent aggregation and ensure optimal dispersion within the composite matrix. These treated CNTs were then entangled with MoS_2 nanosheets to form layered structures, facilitating the creation of efficient heat transfer pathways. The resulting MoS_2-CNT composites were fabricated using a hot-pressing method, with polyphenylene sulfide (PPS) layers integrated for structural integrity. Through experimental investigation and characterization, our composites exhibited substantial improvements in thermal conductivity, achieving an impressive 5.77 W/mK. Additionally, the incorporation of PPS layers endowed the composites with insulation properties, further enhancing their suitability for diverse applications. Notably, the composite demonstrated a tensile strength of 67 MPa, indicating its potential for structural applications. This research underscores the promising potential of MoS_2-CNT composites in addressing critical challenges in thermal management and structural engineering across various industries, including automotive and electronics. By offering a comprehensive solution that combines enhanced thermal conductivity, mechanical strength, and insulation properties, our composite material opens avenues for innovation in the development of advanced materials for next-generation technologies.

1. Introduction

The current global energy crisis and associated carbon emissions are presenting significant challenges, prompting a growing interest in electric vehicles (EVs) as an alternative to conventional fuel-powered transportation. The performance of EVs, especially regarding fuel consumption, is heavily influenced by the weight of the vehicle undercarriage. Therefore, it has become crucial to identify prosperous materials capable of replacing existing system to reduce weight of vehicles and enhance overall performances. Engineering plastics (EP) have emerged as up-and-coming candidates across various fields, including the automotive sector, because of their advantageous properties such as low cost and weight, ease to process, and water resistance.

However, the broad utilization of EPs has been limited by several weakness. For instance, polyamide has high hygroscopicity, polycarbonate exhibits low chemical stability, polyurethane and polyvinyl chloride are susceptible to extreme temperatures [1–8]. These drawbacks inhibit the extensive use of EPs in diverse fields. Unlike EPs that have these disadvantages, polyphenylene sulfide (PPS) has emerged as a superior high-performance plastic, maintaining good temperature and chemical resistance. Moreover, the melting point of PPS, 275 °C, surpasses that of other EPs, making it a favorable choice for a range of applications.

Nonetheless, PPS exhibits a notable disadvantage in comparison to other EPs: significantly lower thermal conductivity. To focus on this limitation, researchers have explored the incorporation of carbon

* Corresponding author. School of Chemical Engineering, Chung-Ang University, Seoul, 06974, Republic of Korea.
E-mail address: jooheonkim@cau.ac.kr (J. Kim).

https://doi.org/10.1016/j.jmrt.2024.09.253
Received 13 August 2024; Received in revised form 27 September 2024; Accepted 29 September 2024
Available online 30 September 2024
2238-7854/© 2024 The Authors. Published by Elsevier B.V. This is an open access article under the CC BY-NC-ND license (http://creativecommons.org/licenses/by-nc-nd/4.0/).

materials and oxides or nitrides materials, such as aluminum oxide, boron nitride, or aluminum nitride into PPS matirx to improve its mechanical and thermal properties [9–12]. Previous studies by our group demonstrated that PPS/glass fiber composites utilizing 3-mercaptopropyltrimethoxysilane-treated graphene oxide and polysiloxane-coated aggregated boron nitride achieved a thermal conductivity of 1.18 W/m·K [13]. Tantug et al. [14] reported a PPS composite containing 50% synthetic graphite, attaining a thermal conductivity of 1.65 W/m·K which measured with through-plane direction, 470 % greater than thermal conductivity of pure PPS. Similarly, Shi et al. [15] presented a PPS/PDA-CNTs-SiC composite with polydopamine treatment achieving a through-plane thermal conductivity of approximately 1 W/m·K at a 22% filler ratio. However, there is still room for improvement in the thermal conductivity of PPS composites, and also, the injection molding process presents limitations, with filler loading limits typically capped at 60–70% due to the increasing viscosity. To overcome the limitations of filler loading in injection molding, we selected a hot-pressing method for fabricating layer-by-layer-structured PPS composites. The hybrid filler layer, comprising molybdenum disulfide (MoS_2) and carbon nanotubes (CNTs), was first fabricated without the PPS matrix, and then PPS layers were fabricated on the upper and lower sides of the composites. MoS_2 shows excellent mechanical properties along with a thermal conductivity of 2 W/m·K in the through-plane direction, and 80–100 W/m·K in the in-plane direction [16,17]. CNTs were used to entangle the MoS_2 sheet and create a heat pathway in the through-plane direction, achieving a notable thermal conductivity of 3000 W/mK [18]. However, in the absence of surface treatment the CNTs self-aggregated, requiring acid treatment to attach sulfonate functional groups to their surfaces.

In this study, we aimed to develop composite materials integrating MoS_2 and CNTs with enhanced thermal conductivities. MoS_2 is a two-dimensional (2D) material that has garnered significant attention in the field because of its remarkable electrical and mechanical properties. However, its layered structure limits its thermal conductivity properties. On the other hand, CNTs exhibit excellent thermal conductivity, but face challenges with regard to mixing and dispersion. As such, in this study, we combined MoS_2 with CNTs to create composite materials with complementary properties. However, due to the high viscosity of PPS, it is difficult to manufacture high filling ratios of more than 70% by using extrusion and injection molding processes. And the injection molding method has difficulty in forming a thermal path to increase the thermal conductivity inside the composite. To solve these problems, a sandwich composite was set up to improve the thermal conductivity. The middle layer of MoS_2/CNT not only helps to form a thermal path to achieve high thermal conductivity, but also can achieve a high filler ratio by controlling the amount of the upper and lower PPS layers. The upper and lower PPS layers also help to secure the insulation of the composite material. Since problems such as leakage may occur when current flows through the composite material, securing the insulation of the composite material is an important issue. Therefore, by forming the PPS layer, the thermal conductivity was slightly reduced, but insulation was secured. The synthesis, surface treatment, mixing, and fabrication of our MoS_2-CNT composites were experimentally investigated and characterized. This study is anticipated to contribute to the development of new method for use in thermal management and structural applications, thereby addressing important challenges across various industries.

2. Experimental

2.1. Materials

Polyphenylene sulfide (PPS), sodium molybdate dihydrate ($Na_2MoO_4{\cdot}2H_2O$; 99.5%), thioacetamide (CH_3CSNH_2; reagent grade, 98%), tungstosilicic acid ($H_4(W_{12}SiO_{40})$; 99.9%) were purchased from Sigma-Aldrich. Sodium hydroxide (NaOH, 97%, pellet) and sulfonic acid (H_2SO_4; 98%) were acquired from Daejung Chemical and Metals Co., Ltd. (Seoul, Korea). CNTs were purchased from Carbon Nano-Material Technology Co., LTD. (Pohang, Korea). All reagents were used as received without further purification.

2.2. Preparation of MoS_2/CNT hybrid filler

Fig. 1 shows overall schematic process for fabricating PPS/MoS_2/CNT composites. The details for synthesis of MoS_2, exfoliation of MoS_2, acid-treatment of CNT and hot-pressing process can be found below.

The synthesis process of MoS_2 was used in previously reported study [19]. 0.363 g of sodium molybdate dihydrate and 0.33 g of thioacetamide were taken and completely dissolved in 50 mL of distilled water. And then, 0.403 g of tungstosilicic acid was added into the solution with vigorous magnetic stirring. A 100 mL stainless steel autoclave with a Teflon lining was used to tightly seal a 50 mL reaction solution. The autoclave was maintained at a temperature of 220 °C for 24 h. The resulting black precipitate was filtered and washed several times with NaOH solution, ethanol, and distilled water. It was then dried under vacuum at 60 °C overnight.

1g of CNT was dispersed in 200 ml sulfonic acid at 60 °C for 24 h. The solution was washed with distilled water several times to remove acid, and then dried in a vacuum at 60 °C for overnight. The product was named as AT-CNT.

Liquid exfoliation was performed using a probe sonicator (Sonics & Materials, VCX-750) at a sonication power of 400 W for 4 h. To prevent overload of probe sonication, sonication was performed for 3 h by repeating 3 s of operation and 1 s of rest. The solvent used for sonication was acetone. The exfoliated MoS_2 was named e-MoS_2. MoS_2 and AT-CNT were dispersed together in acetone to exfoliate MoS_2 and at the same time disperse AT-CNT uniformly.

2.3. Composite fabrication using hot-pressing method

The mixture of MoS_2 and CNT with various CNT contents were transferred into a iron mold and then hot-pressed at 170 °C under 50 MPa for 30 min, and the product was disk-like pellet. To fabricate PPS layer, PPS powder was introduced on the upper side of pellet and hot-pressed at 220 °C under 50 MPa for 30 min and the process was repeated to fabricate PPS layer on the reverse side. The fabricated composite was thermally annealed at 250 °C under nitrogen gas condition.

2.4. Characterization

The crystalline structures of the synthesized MoS_2 nanosheet and CNT was confirmed by using X-ray diffraction (XRD; D8 Advance, AXS Bruker) over a 2θ range of 10–80° at 40 kV and 40 mA at a scan rate of 0.1° s−1 under λ = 0.154056 nm Cu Kα radiation. The binding energies of the MoS_2 and CNT fillers were determined via X-ray photoelectron spectroscopy (XPS; K-Alpha, Thermo UK) using an Al Kα X-ray source (1486.6 eV). The morphology of the fillers and the cross-section of the fabricated composites were investigated using field-emission scanning electron microscopy (FE-SEM; SIGMA). Fourier-transform infrared (FT-IR) spectroscopy (PerkinElmer Spectrum One) was conducted to confirm attachment of functional group on CNT by acid treatment. And Raman spectrometer II (DXR2xi, Thermo) was also used to clarified damage of CNT surface with a near-infrared laser operating at 532 nm and a charge coupled device detector. Thermogravimetric analysis (TGA, TGA-2050, TA Instruments) of CNT and AT-CNT was performed by heating the samples from room temperature (RT) to 800 °C at a rate of 20 °C min−1 under air atmosphere. The mechanical properties of the fabricated composites were measured using a universal testing machine (UTM, 3344Q9465, Instron Co.) at a cross-head speed rate of 1 mm/min. The thermal conductivity (κ) was calculated using the relationship κ = α•ρ•C_p, where ρ, α, and Cp are the pellet density, thermal diffusivity, and specific heat capacity, respectively. The thermal diffusivity was measured using an LFA 447 Nanoflash (NETZSCH) system, and the

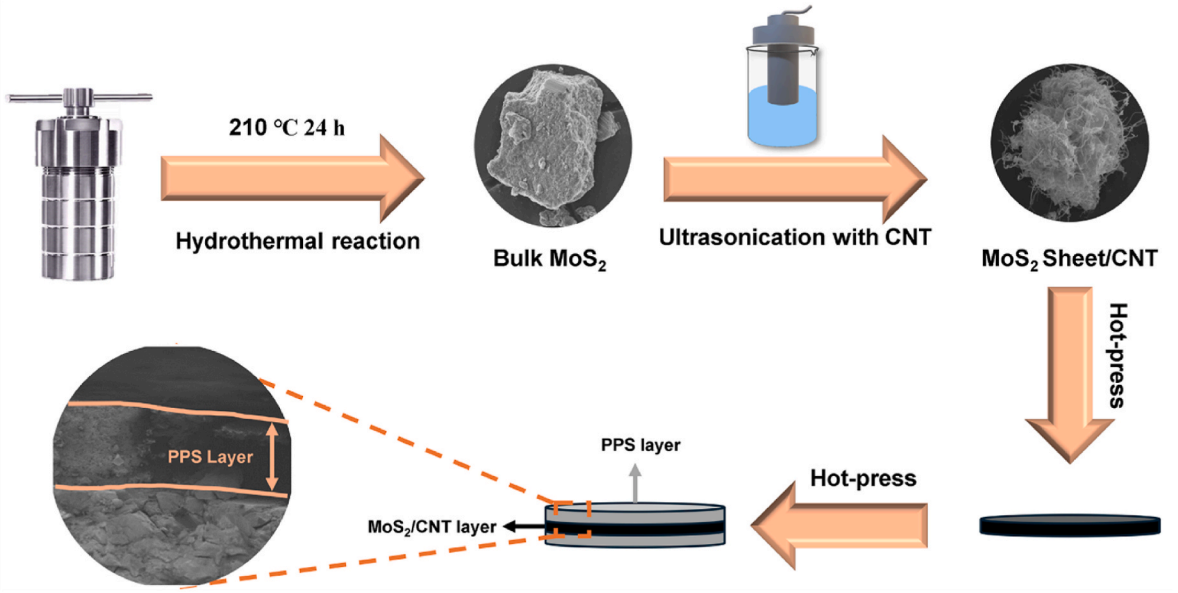


Fig. 1. Schematic illustration of the fabrication process of PPS/MoS_2/CNT composites.

specific heat capacity of the fabricated composites was quantified using differential scanning calorimetry (DSC, DSC-Evo, KEP Tech). The density of the composites was calculated using Archimedes' method. The electrical resistance of the composites were calculated using the four-point probe method.

3. Results and discussion

The synthesis, exfoliation, and morphology of the MoS_2 sheets were verified by XRD, FE-SEM, and XPS. The XRD pattern of MoS_2 (Fig. 2(a)) confirmed the synthesis of MoS_2, which corresponding to the previous study (PDF #37–1492) [20]. When the nanosheet structure consisted of only a few layers, the XRD pattern showed a broadening of the diffraction peaks. Specifically, characteristic peaks were observed at 33° indicating (100) plane, 38° indicating (103) plane, and 59° indicating (110) plane of the MoS_2 nanosheets. The corresponding FE-SEM images (Fig. 2(b) and (c)) showed MoS_2 particles. While the MoS_2 particles did not exhibit a nanosheet structure, the MoS_2 nanosheets aggregation with sizes of few nanometers can be confirmed by high-resolution FE-SEM images. In Fig. 2(d) and (e), the Mo 3d and S 2p XPS spectra indicated

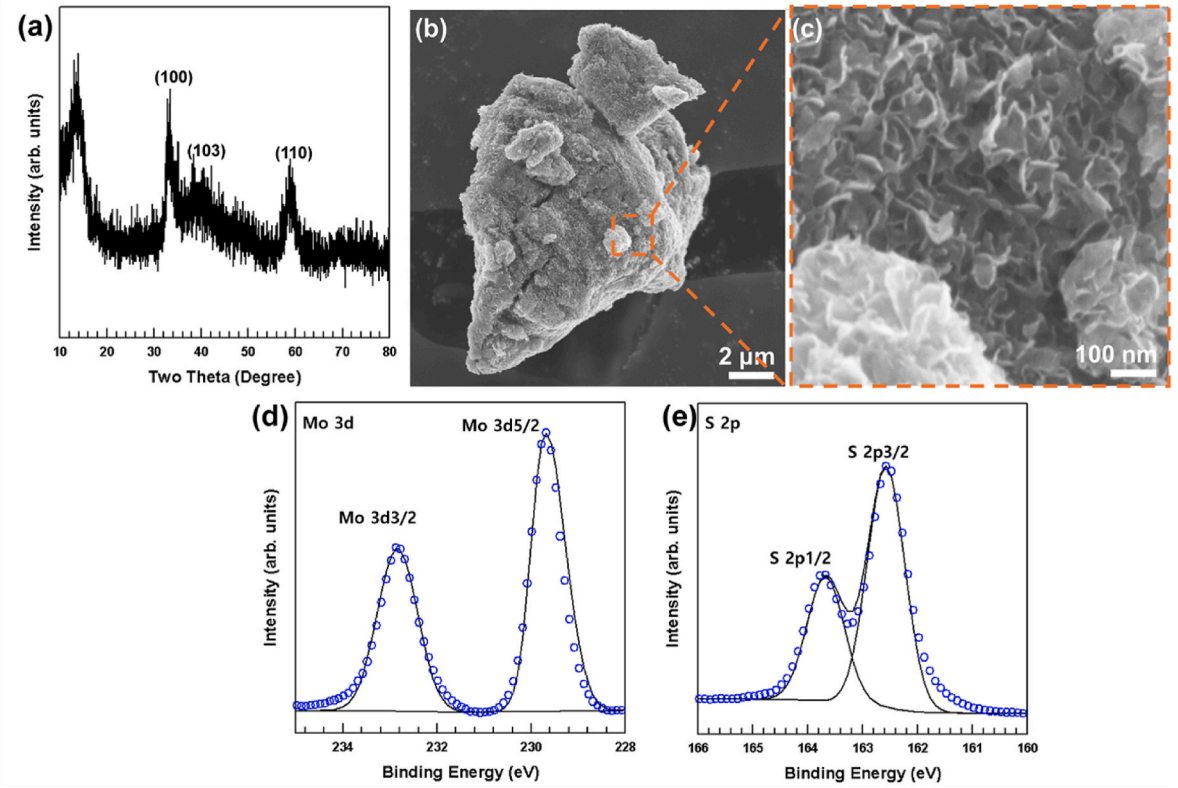


Fig. 2. (a)XRD pattern (b) FE-SEM (c) High-resolution FE-SEM image of MoS_2. XPS (d) Mo 3d deconvolution and (e) S 2p deconvolution of MoS_2.

the successful synthesis of MoS_2 nanosheets with spin–orbit components difference of 3.15 eV. The Mo 3d5/2 peak at 229.5 eV illustrated Mo was in the Mo^{4+} state. Additionally, the S 2p3/2 peak at 162.4 eV corresponds to previous results on MoS_2 [21]. Based on these results, MoS_2 was successfully synthesized via the hydrothermal reaction.

Subsequently, the synthesized MoS_2 underwent exfoliation via liquid-phase exfoliation (LPE) using ultrasonication. The layers were peeled from the bulk material through prolonged sonication. The crystal structure of MoS_2 resembled that of graphene; hence, it formed stacked 2D sheet layers, with a low interlayer van der Waals force, facilitating easy peeling. Owing to the high power and long duration of the ultrasonication process, the occurrence of MoS_2 oxidation must be verified. The characterization results for the exfoliated MoS_2 (e-MoS_2) are shown in Fig. 3. By comparing the XRD and XPS results for MoS_2 and e-MoS_2, it was confirmed that the MoS_2 particles underwent no oxidization during ultrasonication. The XRD pattern did not show any additional peaks, such as MoO_2 or MoO_3, while the XPS results indicated only the presence of MoS_2-related peaks in the Mo 3d and S 2p regions, without any shift. Moreover, the FE-SEM images of e-MoS_2 confirmed the successful peel-off of the bulk MoS_2 layers during the ultrasonication process.

CNTs, serving as fillers with high thermal conductivity, were entangled with e-MoS_2 to form layered structures. When the CNT and e-MoS_2 were mixed without any surface treatment, the CNTs aggregated with each other. To prevent this, acid treatment of the CNT (AT-CNT) was performed. The FT-IR results of the CNT and AT-CNT samples (illustrated in Fig. 4(a)) show that the –OH and –SO_3 functional groups were attached to the CNT surfaces. This surface treatment was confirmed using Raman spectroscopy (refer to Fig. 4(b)). The ID/IG ratio of AT-CNT increased from 0.95 to 1.0, owing to the increase in carbon defects with acid treatment. Fig. 4(c–e) comparatively illustrates the XPS results before and after acid treatment of the CNTs. The XPS C 1s spectra of the CNT showed multiple peaks located at 284.7, 285.2, 286.6, 288.3 and 289.1 eV, corresponding to C=C, C–C/C–H, C–OH/C–*O*–C, C=O, and O–C=O bonds, respectively [22]. Post acid treatment, the XPS C 1s spectrum showed an additional peak at 285.3 eV, attributed to C–S bonding [23]. This result indicated the successful attachment of the sulfonate functional group to the CNT surface. The same result was observed in the XPS S 2p spectra of the AT-CNT. The XPS S 2p3/2 peak at 169 eV corresponds to the sulfate functional group, wherein a spin-orbit splitting with a difference of 1.16 was observed. The TGA results (illustrated in Fig. 4(f)) indicated the successful acid treatment of the CNT surface. The pristine CNT sample exhibited high thermal stability up to 600 °C, after which weight loss manifested gradually, with a decrease to 10%. In contrast, AT-CNT demonstrated degradation up to 300 °C due to the presence of sulfonate functional groups on the surfaces, resulting in an earlier onset of weight loss compared to pristine CNT. Notably, acid treatment did not alter the crystal structure of the CNT, as evidenced by the XRD patterns in Fig. 4(g). The XRD pattern of pristine CNT displayed the strongest peak corresponding to the (002) plane [24]. After acid treatment, the XRD pattern was similar to that of the pristine CNT, without the presence of additional peaks. These results indicate that the acid treatment of CNTs can successfully introduce sulfonate functional groups on their surface, without affecting their crystal structure.

The FE-SEM images in Fig. 5 illustrate the morphologies of CNT, AT-CNT, e-MoS_2/CNT and e-MoS_2/AT-CNT. Compared Fig. 5(a) and (b), the surface of CNT became smoother and more dispersion after acid treatment. In Fig. (c–f), as mentioned above, the pristine CNTs aggregated, whereas the AT-CNTs showed good dispersion with MoS_2. It can be seen that the sulfonate functional group on the surface of the CNTs affected the molecular force between MoS_2 and CNT through hydrogen bonding or van der Waals forces, thereby facilitating CNT dispersion. As the CNT ratio increased, the CNTs became more entangled with e-MoS_2, promoting the maintenance of the film during vacuum filtration; however, the film was weak in strength and contained numerous pores. Therefore, a more effective method for fabricating the e-MoS_2/AT-CNT layer

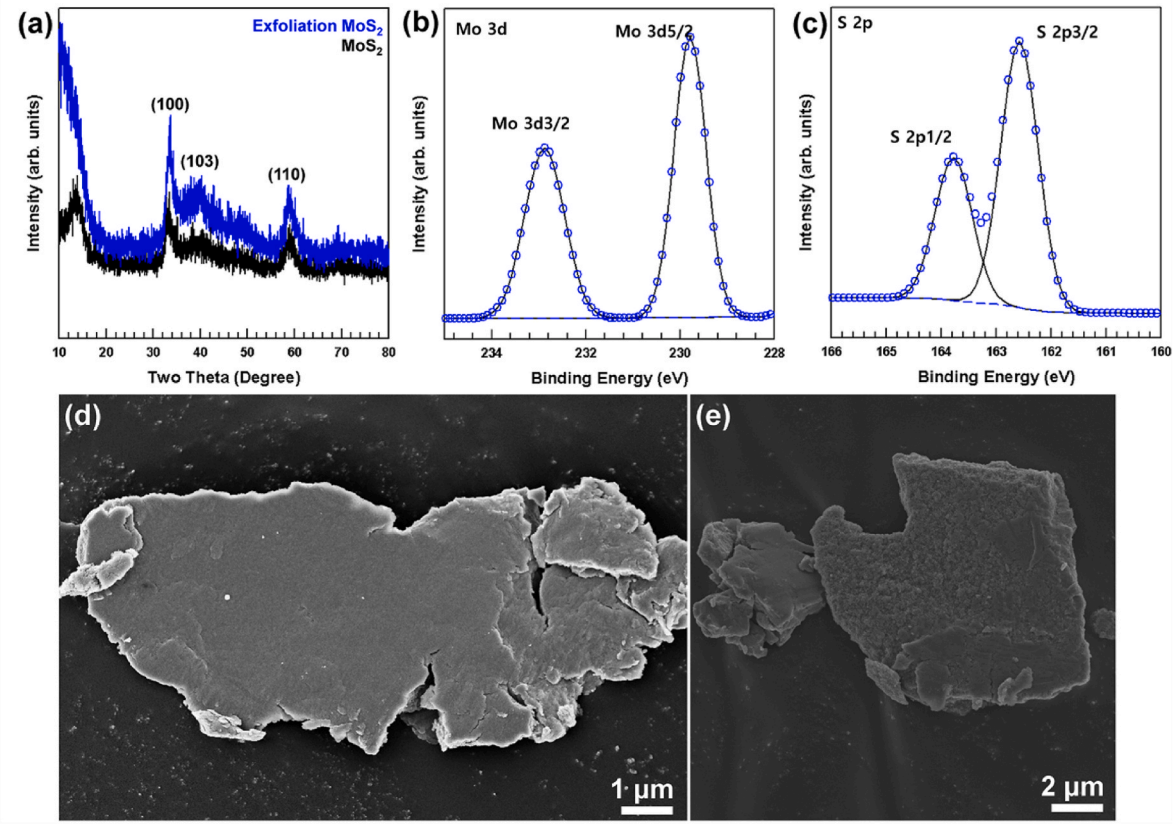


Fig. 3. (a) XRD patterns of MoS_2 and e-MoS_2. XPS (b) Mo 3d deconvolution and (c) S 2p deconvolution of e-MoS_2. (d–e) FE-SEM images of e-MoS_2.

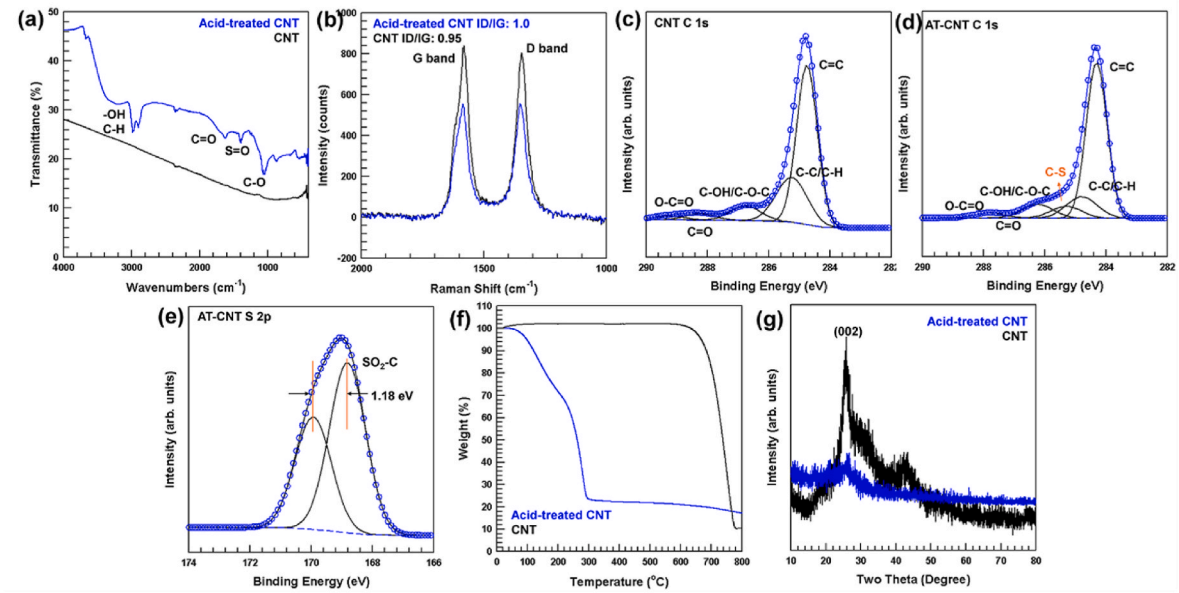


Fig. 4. (a) FT-IR spectra (b) Raman spectra of CNT and AT-CNT. XPS (c) C 1s deconvolution of CNT, (d) C 1s deconvolution and (e) S 2p deconvolution of AT-CNT. (f) TGA analysis and (g) XRD patterns of CNT and AT-CNT.

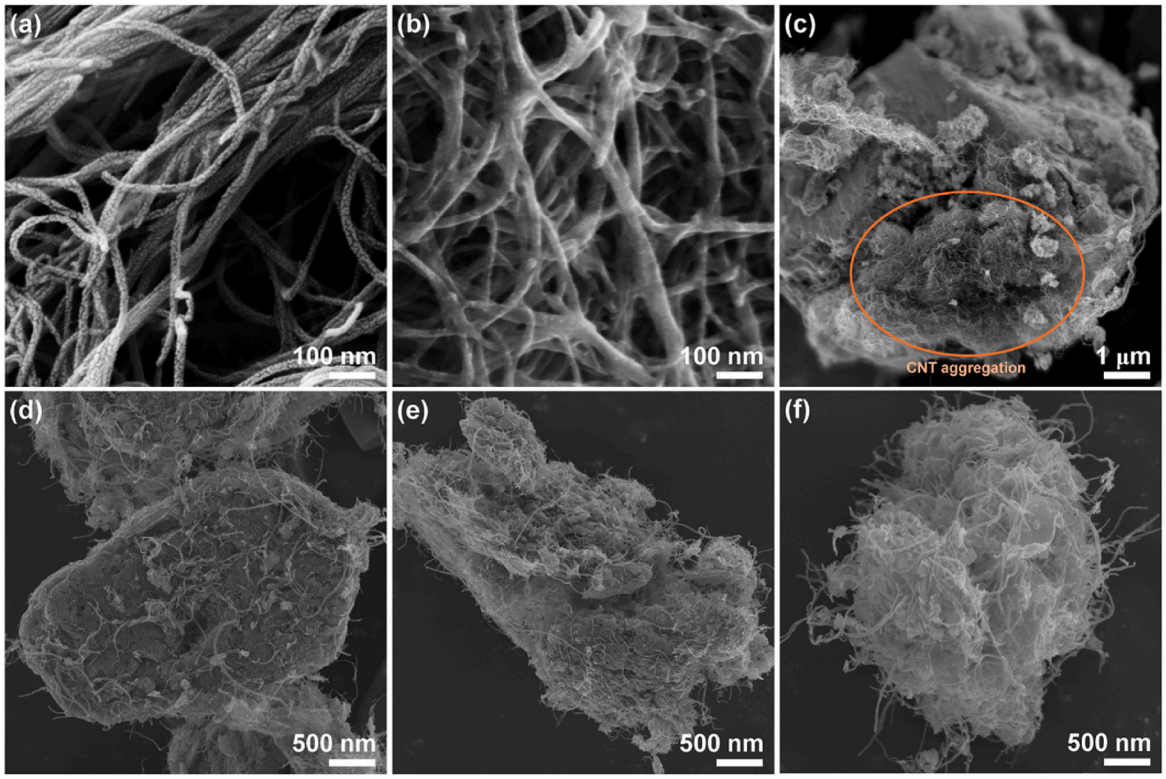


Fig. 5. FE-SEM images of (a) CNT (b) AT-CNT (c) MoS_2/CNT (d) MoS_2/5CNT (e) MoS_2/10CNT and (f) MoS_2/20CNT hybrid fillers.

should be considered. To make the e-MoS_2/AT-CNT sheet, a hot-pressing method was selected, and then the top and bottom of the sheet were coated with PPS to produce a composite with a PPS-MoS_2/CNT-PPS layer structure (refer to Fig. 6). Fig. 6(a) and (b) show cross-sectional FE-SEM image of hot-pressed MoS_2. The MoS_2 disk-shaped composite produced by hot-pressing has a dense shape with a thickness of 1–2 mm. The high-resolution FE-SEM of MoS_2 composite shows that the MoS_2 particles were compressed into a dense bulk material by heat and pressure. The high-resolution FE-SEM images in Fig. 6(c) and (d) illustrate the entangled MoS_2 sheet morphology with the CNTs and the formation of a heat path along the through-plane direction. At a low CNT ratio, the heat path was difficult to determine. In Figs. 6(d), 20 wt% of ATCNT covered MoS_2 surfaces and fabricated through-plane direction heat path. The cross-sectional FE-SEM image in Fig. 6(e) shows a clear layered structure. Compared to the injection molding process, the layered structure of PPS-MoS_2/CNT-PPS increased the ratio of the filler. In previous studies, the production of PPS composite materials using injection molding was challenging because the viscosity increased rapidly as the filler content

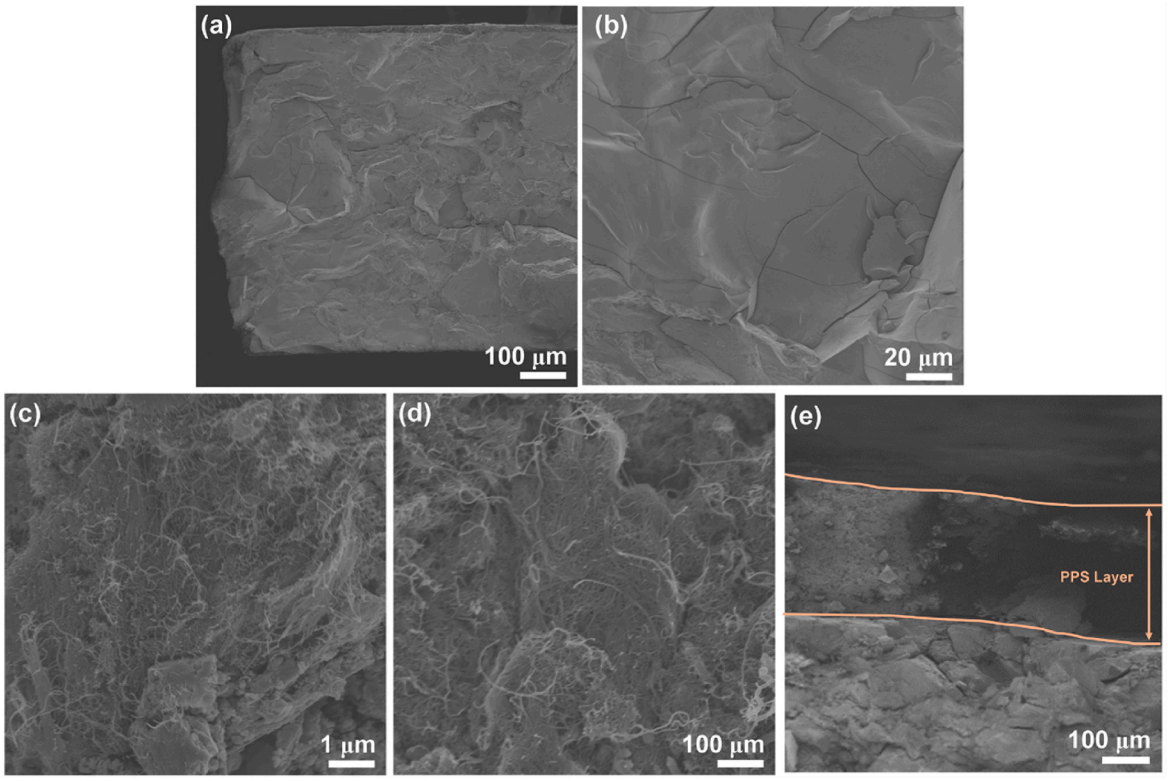


Fig. 6. Cross-sectional FE-SEM images of (a) MoS_2 composite (b) high-resolution MoS_2 composites (c) MoS_2/10CNT composite (d) MoS_2/20CNT composite and (e) PPS/MoS_2/20CNT composite.

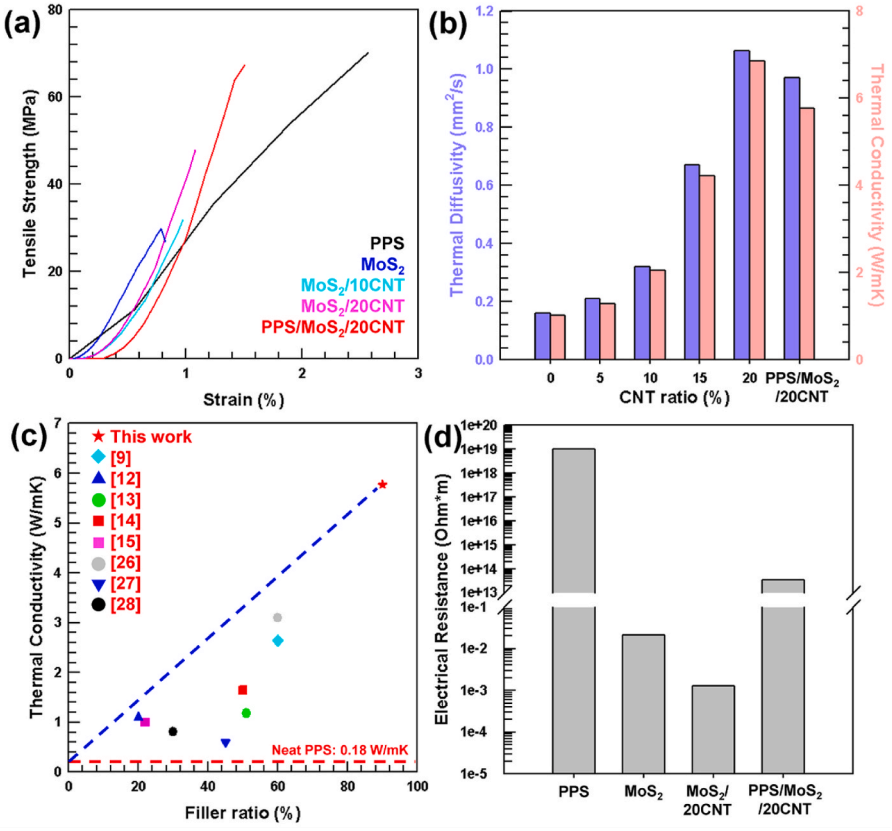


Fig. 7. (a) Tensile strength vs. Tensile strain properties (b) Thermal diffusivity and conductivity (c) Thermal conductivity comparison with reported PPS composites and (d) electrical resistance of the composites.

increased. The manufacturing of composites shows limitations when the filler content exceeds approximately 70 wt%; therefore, in this study, a different approach was adopted to achieve a higher filler content. The filler ratio was calculated as the difference between the weights of the MoS_2/CNT sheet and the PPS-MoS_2/CNT-PPS composites. Using this strategy enabled the fabrication of PPS-MoS_2/CNT-PPS composites with 90% filler ratio. During the hot-pressing process, the pores were compressed and reduced by the high pressure. During the fabrication process of the PPS layers, the pressing temperature was set to 220 °C, which was between the glass temperature (150 °C) and melting point (280 °C) of the PPS. PPS melts during the pressing process to form a layer, wherein a certain amount helps form a dense composite.

The mechanical properties of the composites were measured at RT using a universal testing machine (refer to Fig. 7(a)). The fabricated MoS_2 composite exhibited a low tensile strength of 32 MPa. MoS_2 is known to have very good mechanical properties, but because it was made of a thin composite material with a thickness of 1–2 mm, its mechanical properties were low. With increasing AT-CNT content, the tensile strength increased up to 48 MPa. As seen in the cross-sectional FE-SEM image of the composite material above, as the AT-CNT content increased, the mechanical properties improved by entangling MoS_2. After fabricating PPS layer above and below the MoS_2/CNT, the tensile strength of the composite increased to 67 MPa, originating from PPS's high tensile strength (70 MPa) [25]. However, compared to the PPS composite fabricated using the injection molding process, the tensile strength was weak. This could be explained from the fact that composites manufactured using injection molding are manufactured such that the PPS matrix surrounds all surfaces of the composite, whereas composites manufactured using the hot-pressing method have PPS layers only on the top and bottom surfaces, resulting in relatively reduced mechanical strength.

When the composite material was manufactured by hot pressing, despite the slight decrease in mechanical strength, high thermal conductivity was achieved owing to the high filler content and the formation of through-plane direction heat path. The thermal conductivities of the MoS_2 and CNT components were 80–100 W/mK (in-plane) and 3000 W/mK, respectively. However, owing to anisotropy in the thermal conductivity of MoS_2, its through-plane thermal conductivity was lower than 2 W/mK. This stemmed from the 2D layered crystal structure of MoS_2, wherein MoS_2 layers were stacked with weak van der Waals forces; therefore, the movement of phonons between layers was impeded, resulting in an anisotropic thermal conductivity. To improve the low through-plane thermal conductivity of MoS_2, we entangled it with highly thermally conductive CNTs to fabricate a heat path in through-plane direction. When a composite has many pores, thermal conductivity rapidly decreases due to the low thermal conductivity of air (0.024 W/mK) and phonons can be easily scattered at the pore interfaces. Here, the hot-pressing method was selected to avoid the generation of a porous structure. The measured thermal conductivities of composites with various filler ratios are presented in Fig. 7(b) using LFA 447 Nanoflash (NETZSCH). First, We measured thermal conductivity of MoS_2 and MoS_2/CNT composite without PPS layer. When the CNT ratio increased, the thermal conductivity also increased owing to the formation of a heat path. The formation of heat path can be verified by increasing thermal diffusivity. Due to the lower density of CNT (2.26 g/cm^3) compared to MoS_2 (5.06 g/cm^3), the density of the composite decreased with increasing CNT contents. The thermal conductivity calculation formula is expressed as the product of density, thermal diffusivity, and Cp value. As the CNT content increased, the density decreased, but the thermal diffusivity rapidly increased due to the formation of a heat transfer path in the through-plane direction, resulting in improved thermal conductivity of 6.8 W/mK. Therefore, we set the MoS_2:CNT ratio to 8:2 to fabricate PPS layer. The PPS/MoS_2/CNT composite shows a slightly decreased thermal conductivity of 5.77 W/mK due to the extremely low thermal conductivity of neat PPS, 0.18 W/mK. In Fig. 7(c), We compared recent studies of PPS composites using injection molding process [9,12–15,26–28]. Our results shows high filler loading of 90% and high thermal conductivity of 5.77 W/mK. By considering filler contribution for enhancing thermal conductivity, a linear line was introduced, which connect thermal conductivity of neat PPS (filler ratio: 0%) and 5.77 W/mK (filler ratio: 90%). The slope of the introduced line contributes to the increase in thermal conductivity per 1% of filler, and it can be seen that it has a high slope compared to existing literature. From this, it can be said that our research achieved a high filler content and at the same time achieved a more effective improvement in thermal conductivity compared to the injection molding method. The thermal conductivity was slightly reduced with the introduction of the PPS layer, however the introduction of PPS made it possible to have insulation properties as shown in Fig. 7(d). The electrical resistance of MoS_2 shows 0.0214 Ω m, which indicates MoS_2 is highly electrically conductive material. With CNT content of 20%, the electrical resistance decreased to 1.3×10^{-3} Ω•m. When thermal interface materials have insulating properties, the insulating layer can be removed from automotive parts, which helps reduce the weight of the parts. Insulating performance is also an important issue when considering high-voltage battery packs for electric vehicles. By considering this issue, with introducing PPS layers, the electrical resistance sharply increased to 3.46×10^{13} Ω•m, which can be seen insulating material. Considering both thermal, mechanical and insulating properties, our composite with a MoS_2/CNT ratio of 8:2 and filler/PPS ratio of 9:1 exhibited excellent performance, achieving a thermal conductivity of 5.77 W/mK and a tensile strength of 67 MPa with insulating property.

4. Conclusions

In conclusion, in this study we successfully synthesized and characterized MoS_2 nanosheets through a hydrothermal reaction, followed by liquid-phase exfoliation to produce exfoliated MoS_2 (e-MoS_2). The characterization results confirm the successful synthesis and exfoliation of MoS_2 without oxidation during ultrasonication. Furthermore, carbon nanotubes (CNTs) were surface-treated with acid to enhance dispersion and entangled with e-MoS_2 to form layered structures. The acid treatment of the CNTs was confirmed by spectroscopic and thermal analyses. The resulting MoS_2/CNT and MoS_2/acid-treated CNT (AT-CNT) composites exhibited different morphologies, with AT-CNT showing improved dispersion owing to the sulfonate functional groups on their surfaces. A hot-pressing method was employed to fabricate PPS-MoS_2/CNT-PPS composites with a high filler content and layered structure. Despite the slightly reduced mechanical strength compared to injection molding, the composites demonstrated enhanced thermal conductivity, which was attributed to the high filler content and the formation of heat paths. By optimizing the MoS_2/CNT and filler/PPS ratios, a composite with balanced thermal and mechanical properties was obtained, with a thermal conductivity of 5.77 W/mK and a tensile strength of 67 MPa. Overall, this study indicates a promising approach for fabricating engineering plastic-based composite materials with improved thermal conductivity and mechanical strength that hold the potential for various applications in thermal management and structural materials without melt extrusion process.

Data availability statement

The raw/processed data required to reproduce these findings cannot be shared at this time as the data also forms part of an ongoing study.

Declaration of competing interest

The authors declare that they have no known competing financial interests or personal relationships that could have appeared to influence the work reported in this paper.

Acknowledgments

This research was supported by the Industrial Technology Innovation Program (20011165) funded by the Ministry of Trade, Industry & Energy (MOTIE, Korea) and funded and conducted under the Competency Development Program for Industry Specialists of the Korean Ministry of Trade, Industry and Energy (MOTIE), operated by Korea Institute for Advancement of Technology (KIAT) (No. P0012453, Next-generation Display Expert Training Project for Innovation Process and Equipment, Materials Engineers).

References

[1] Jang K-S. Mechanics and rheology of basalt fiber-reinforced polycarbonate composites. Polymer 2018;147:133–41.
[2] Kausar A. A review of filled and pristine polycarbonate blends and their applications. J Plast Film Sheeting 2018;34:60–97.
[3] Francisco DL, Paiva LB, Aldeia W. Advances in polyamide nanocomposites: a review. Polym Compos 2019;40:851–70.
[4] García JM, García FC, Serna F, de la Peña JL. High-performance aromatic polyamides. Prog Polym Sci 2010;35:623–86.
[5] Fabbri P, Bassoli E, Bon SB, Valentini L. Preparation and characterization of poly (butylene terephthalate)/graphene composites by in-situ polymerization of cyclic butylene terephthalate. Polymer 2012;53:897–902.
[6] Joshi M, Misra A, Maiti S. Polybutylene terephthalate/high-density polyethylene alloys. I. Morphological studies. J Appl Polym Sci 1991;43:311–28.
[7] Janik H, Marzec M. A review: fabrication of porous polyurethane scaffolds. Mater Sci Eng C 2015;48:586–91.
[8] Moulay S. Chemical modification of poly (vinyl chloride)—still on the run. Prog Polym Sci 2010;35:303–31.
[9] Gu J, Guo Y, Yang X, Liang C, Geng W, Tang L, Li N, Zhang Q. Synergistic improvement of thermal conductivities of polyphenylene sulfide composites filled with boron nitride hybrid fillers. Compos. A: Appl. Sci. Manuf. 2017;95:267–73.
[10] Jiang Y, Liu Y, Min P, Sui G. BN@ PPS core-shell structure particles and their 3D segregated architecture composites with high thermal conductivities. Compos Sci Technol 2017;144:63–9.
[11] Çoban O, Bora MÖ, Sinmazçelik T. Effect of mixed size particles reinforcing on the thermal and dynamic mechanical properties of A l2 O 3/PPS composites. Polym Compos 2016;37:3219–27.
[12] Kim M, Park S, Park J. Effect of the grafting reaction of aluminum nitride on the multi-walled carbon nanotubes on the thermal properties of the poly (phenylene sulfide) composites. Polymers 2017;9:452.
[13] Kim M, Cho Y, Yang W, Kim J. Improved thermal conductivity of poly (p-phenylene sulfide)/glass fiber composites via addition of polysiloxide-coated aggregated boron oxide and silane-treated graphene oxide. Mater Chem Phys 2023; 302:127737.
[14] Tantug GS, Seki Y, Sarikanat M, Altay L, Gulen S, İsbilir A. Thermal conductivity and mechanical properties of synthetic graphite loaded polyphenylene sulfide composites. Proceedings of the 35th international conference of the polymer processing society (PPS-35). AIP Publishing; 2020, 20033.
[15] Shi Y, Bai Y, Lei Y, Zhang H, Zhou S, Zou H, Liang M, Chen Y. Simultaneously enhanced heat dissipation and tribological properties of polyphenylene sulfide-based composites via constructing segregated network structure. J Mater Sci Technol 2022;99:239–50.
[16] Gandi AN, Schwingenschlögl U. Thermal conductivity of bulk and monolayer MoS2. Europhys Lett 2016;113:36002.
[17] Li W, Carrete J, Mingo N. Thermal conductivity and phonon linewidths of monolayer MoS2 from first principles. Appl Phys Lett 2013;103.
[18] Kumanek B, Janas D. Thermal conductivity of carbon nanotube networks: a review. J Mater Sci 2019;54:7397–427.
[19] Chaudhary N, Khanuja M, Islam S. Hydrothermal synthesis of MoS2 nanosheets for multiple wavelength optical sensing applications. Sens Actuators, A 2018;277: 190–8.
[20] Singh MK, Chettri P, Tripathi A, Tiwari A, Mukherjee B, Mandal R. Defect mediated magnetic transitions in Fe and Mn doped MoS 2. Phys Chem Chem Phys 2018;20: 15817–23.
[21] Pacholik G, Enzlberger L, Benzer A, Rameshan R, Latschka M, Rameshan C, Föttinger K. In situ XPS studies of MoS2-based CO2 hydrogenation catalysts. J Phys D Appl Phys 2021;54:324002.
[22] Okpalugo T, Papakonstantinou P, Murphy H, McLaughlin J, Brown N. High resolution XPS characterization of chemical functionalised MWCNTs and SWCNTs. Carbon 2005;43:153–61.
[23] Chin HC. Preparation and characterization of carbon-sulfur surface compounds. Carbon 1981;19:175–86.
[24] Irshad A, Shahid M, El-Bahy SM, El Azab IH, Mersal GA, Ibrahim MM, Agboola PO, Shakir I. Nickel doped CoAl2O4@ CNT nanocomposite: synthesis, characterization, and evaluation of sunlight driven catalytic studies. Phys B Condens Matter 2022; 636:413873.
[25] Garrell MG, Ma B-M, Shih AJ, Lara-Curzio E, Scattergood RO. Mechanical properties of polyphenylene-sulfide (PPS) bonded Nd–Fe–B permanent magnets. Mater Sci Eng, A 2003;359:375–83.
[26] Ryu S, Kim K, Kim J. Silane surface modification of boron nitride for high thermal conductivity with polyphenylene sulfide via melt mixing method. Polym Adv Technol 2017;28:1489–94.
[27] Zhao J, Cai S, Chen X, Ren H, Yan Y. Preparation and properties of boron nitride or aluminum nitride reinforced glass fiber/modified polyphenylene sulfide composites. Adv Polym Technol 2023:2023.
[28] Guo B, Lin Q, Zhao X, Zhou X. Crystallization of polyphenylene sulfide reinforced with aluminum nitride composite: effects on thermal and mechanical properties of the composite. Iran Polym J (Engl Ed) 2015;24:965–75.